Journal of Environmental Management 407 (2026) 129845

Contents lists available at ScienceDirect

Journal of Environmental Management

journal homepage: www.elsevier.com/locate/jenvman

Research article

Short-term recovery of urban soil functions after de-sealing in Palermo (Italy)

Riccardo Scalenghe *, Monica Auteri, Dario Autovino, Giorgio Baiamonte, Giacomo Belvisi, Chiara Cappadonia, Gaetano Caltabellotta, Alessandra Carrubba, Giuseppe Ciraolo, Antonio Comparetti, Giuseppe Di Miceli, Matteo Ippolito, Dario De Caro, Massimo Iovino, Nicoletta Lala, Santo Orlando, Filippo Saiano, Mauro Sarno, Luca Settanni, Luciano Gristina

Università degli studi di Palermo, Palermo, Italy

ARTICLE INFO

Keywords:
Soil sealing
Urban soil
Technosol
Infiltration
Albedo
Microbial activity
Mediterranean

ABSTRACT

Urban soil sealing impairs stormwater regulation, microclimate and biological activity, yet field evidence on how newly de-sealed soils evolve in Mediterranean cities remains scarce. We report a 24-month experiment in Palermo (Italy) on a long-sealed parking-lot Technosol where asphalt was removed and four surface treatments were compared: two unvegetated crushed-asphalt options and two vegetated soil-rehabilitation treatments with imported topsoil. We monitored steady-state Beerkan infiltration, soil cone penetrometer resistance, vegetation dynamics, CO_2 efflux, microbial loads and spectral properties relative to conditions one week after de-sealing (time 0). Immediately after asphalt removal, all plots showed extremely high infiltration, typical of structureless coarse rubble. By 18 months, steady-state infiltration had declined by 25–97% relative to the initial measurement and diverged among treatments: vegetated rehabilitation plots exhibited the strongest proportional reductions and longest run times, while unvegetated crushed-asphalt surfaces retained much higher infiltrability. Cone resistance in previously compacted sublayers fell by around an order of magnitude relative to pre-de-sealing values, approaching ranges favourable for root growth. Vegetation established more rapidly and densely in rehabilitated plots, which also showed higher microbial loads and CO_2 efflux than crushed-asphalt surfaces and sealed controls, indicating rapid reactivation of soil biological functioning. Surface albedo increased relative to asphalt as vegetation developed, suggesting co-benefits for local heat-stress mitigation. Overall, our results show that micro-de-sealing can transform sealed rubble into functional soil–plant systems within a few years, but hydrological and biological trajectories depend strongly on surface design and vegetation choice.

1. Introduction

Urban expansion has been accompanied by extensive soil sealing, whereby natural or managed soils are covered by asphalt, concrete or other impervious materials (Nizeyimana et al., 2001; Scalenghe and Ajmone-Marsan, 2009; Romero Díaz et al., 2017; Siedentop and Fina, 2012). This process alters hydrological partitioning, disrupts soil biological activity and carbon cycling, and reduces the capacity of cities to manage stormwater and heat stress (Hopkins et al., 2015; Pistocchi et al., 2015; Recanatesi et al., 2017; Kabisch and Haase, 2013). These impacts are particularly acute in Mediterranean cities, where intense rainfall events coincide with high levels of impervious cover and limited stormwater infrastructure, amplifying flood and heat-risk in densely built neighbourhoods (Maienza et al., 2021; Ugolini et al., 2020).

Over the past two decades, considerable attention has been paid to mapping sealed surfaces and quantifying their extent and growth (Criado et al., 2020; García and Pérez, 2016;Elvidge et al., 2007; García Alvarado et al., 2018; Peroni et al., 2020; Tardieu et al., 2021). Most studies have focused on the two-dimensional spread of impervious cover, often using remote sensing indicators or land-use metrics, and only rarely have they examined how sealing and de-sealing affect the underlying soil body in three dimensions (Krówczyńska et al., 2016;

* Corresponding author.
E-mail address: riccardo.scalenghe@unipa.it (R. Scalenghe).

https://doi.org/10.1016/j.jenvman.2026.129845
Received 24 December 2025; Received in revised form 10 April 2026; Accepted 27 April 2026
Available online 5 May 2026

Pabjanek et al., 2017; Pérez and García, 2016; Aristegui and Perez, 2017). Yet the consequences of sealing for soil functions depend strongly on the properties of the pre-existing soil, the nature of the anthropogenic materials added, and the depth and continuity of the sealing layers (IUSS WG WRB, 2006; 2022; Calzolari et al., 2020). Urban Technosols derived from long-term sealing can differ markedly in structure, porosity and artefact content from nearby unsealed soils, with direct implications for infiltration, storage and rooting depth once sealing is removed (Ajmone-Marsan and Biasioli, 2010; Ajmone-Marsan et al., 2019; Howard et al., 2013; Howard and Olszewska, 2011).

In parallel, de-sealing has emerged as a practical strategy in urban planning and environmental policy and is increasingly discussed in European and national frameworks as part of wider efforts to limit, mitigate and compensate soil sealing (Prokop et al., 2011; European Commission, 2012, 2013; Stankovics et al., 2018). Removing or perforating paved surfaces and rehabilitating the soil beneath is promoted as a nature-based solution for managing stormwater, reducing urban heat, and improving liveability in compact cities, with several municipalities issuing guidelines and programmes for the regeneration of sealed plots and the reuse of topsoils (Canino et al., 2020; Graie, 2018; Vieillard et al., 2024; Kabisch and Haase, 2013). However, practical guidance on how de-sealed soils behave over time, and how fast they recover key functions, remains scarce (Louise et al., 2024). Most of the available evidence concerns permeable (or pervious) pavements and other engineered stormwater devices, where infiltration is delivered by a deliberately designed aggregate–geotextile–subbase system (Maienza et al., 2021; Ugolini et al., 2020; Rodríguez-Rojas et al., 2018; Fokaides et al., 2016). By contrast, de-sealing exposes a legacy soil body—often a long-sealed Technosol with heterogeneous artefact-rich fills—whose structure, contaminant context, and biological potential were not engineered for infiltration in the first place (IUSS Working Group WRB, 2022; Calzolari et al., 2020). As a result, the post-intervention trajectory of the soil body itself after de-sealing—especially under Mediterranean climates and on long-sealed Technosols—remains rarely documented (Fini et al., 2017; O'Riordan et al., 2021; Sandin et al., 2018).

Several specific knowledge gaps limit the integration of soil-centred de-sealing into urban environmental management. First, the short- to mid-term evolution of infiltration capacity and soil physical status after seal removal is poorly constrained, even though hydrological planning tools often assume that post-intervention soils can approximate pre-sealing hydraulic conditions (Hopkins et al., 2015; Pistocchi et al., 2015; Recanatesi et al., 2017). Immediately after removing an impervious layer, the exposed material can behave like a coarse, structureless aggregate, with a transient “hyper-permeable” state whose rate of moderation toward more soil-like behaviour is largely unknown (Sandin et al., 2018). Second, there is limited field evidence on how low-disturbance surface options—such as retaining crushed asphalt, adding simple organic amendments, or replacing only a thin upper layer with topsoil—shape the recovery of biological activity and vegetation, despite the well-documented effects of sealing on pH, redox conditions and the redistribution of potentially toxic elements in urban soils (Ajmone-Marsan and Biasioli, 2010; Ajmone-Marsan et al., 2019; Martinová et al., 2016). Third, the coupling between subsurface recovery and surface radiant properties (albedo and related thermal behaviour) remains under-explored, even though these properties underpin microclimate regulation and heat mitigation benefits of urban greening (Fokaides et al., 2016; Tardieu et al., 2021).

Addressing these gaps requires tightly controlled field experiments that compare alternative de-sealing designs within the same soil body. Urban Technosols can vary “handful by handful” in texture, artefact content and structure, with direct consequences for hydrological and biogeochemical responses (IUSS Working Group WRB, 2022; Calzolari et al., 2020). Minimising initial-condition differences, even at the cost of limited spatial replication, therefore enables clearer process attribution and, critically, allows the co-evolution of physical, biological and radiative indicators to be assessed in parallel over time (Sandin et al., 2018). This design was therefore intended to maximise comparability among treatments rather than to represent the full diversity of urban Technosols; accordingly, the results should be interpreted as process-level evidence from a controlled case study, to be tested in future multi-site investigations spanning a wider range of urban fill histories and substrate conditions.

Our objectives were to (i) quantify the short- to mid-term trajectory of infiltration capacity and key physical properties after de-sealing under contrasting low-disturbance surface designs; (ii) test whether vegetated versus non-vegetated options differentially accelerate biological recovery and vegetation development; and (iii) evaluate whether subsurface recovery is expressed in measurable shifts in surface radiative properties relevant to urban microclimate regulation. We tested three hypotheses: H1, immediately after de-sealing, all treatments exhibit very high steady-state infiltration that declines over time; H2, vegetated rehabilitation treatments (RA1, RA2) accelerate the transition from hyper-permeability to moderated infiltration and lower penetration resistance relative to CA and CAOM; and H3, vegetated rehabilitation treatments increase microbial load, CO_2 efflux, vegetation development, and surface albedo relative to crushed-asphalt treatments and sealed controls (e.g., Fini et al., 2017; O'Riordan et al., 2021).

The experiment is intentionally local in scope: all plots were established within a single long-sealed Technosol body to avoid confounding treatment effects with differences in parent material or fill history (IUSS Working Group WRB, 2022; Calzolari et al., 2020). While this constrains spatial generalisation, it provides a robust, process-level comparison of de-sealing options under realistic field conditions in a Mediterranean city, directly informing the design of soil-centred de-sealing interventions for stormwater and climate adaptation.

2. Material and methods

The study area is approximately 750 m^2, of which about 470 m^2 are occupied by a single-storey building. The remaining part was paved with about 15 cm of asphalt in 1968, i.e. several decades before the de-sealing intervention described here. About 170 m^2 were left unpaved. Light vehicles have been driven through and parked throughout this area.

Although compacted by use, the unpaved soil is similar to the surrounding soil, which has been used for experimental cultivation of both tree and herbaceous species since the 1960s. Using an old denomination, it is a 'Terra Rossa' soil, which becomes a Technosol after sealing (Fig. SI). Starting from October 2022, a rectangular area of approximately 15 by 5 m was delimited for the first de-sealing experiment. On March 7, 2023, 16 circular areas were de-sealed.

In this experiment, for reasons mainly related to the modelling of fluid dynamics through the soils, the de-sealing geometries are not comparatively tested. The asphalt pavement was removed from circular areas 1 m in diameter (0.785 m^2) and crushed with a pneumatic hammer. To maximise internal validity, all 16 plots were established within the same long-sealed Technosol body; this design reduces confounding from small-scale heterogeneity in urban fills, but necessarily limits broad spatial representativeness. Four post–de-sealing management options were then tested (four replications each; Fig. SI), selected a priori to represent a management-intensity gradient (from minimal intervention with maximum on-site reuse to assisted rehabilitation), consistent with current de-sealing guidance and municipal programmes promoting modular interventions, reuse of materials/topsoils where possible, and nature-based multifunctionality (European Commission, 2012, 2013; Graie, 2018; Canino et al., 2020; Vieillard et al., 2024). These treatments were not intended to reproduce the exact frequency of specific retrofitting options in current practice; rather, they were selected as realistic experimental archetypes spanning a gradient of intervention intensity. To our knowledge, no harmonised evidence base currently quantifies the proportion of these specific options across de-sealing projects in a directly comparable manner, so we intentionally limit our interpretation to relative feasibility and functional

performance. Specifically, the de-sealed area was filled/managed as: (a) crushed asphalt [CA], representing the lowest-input option ("do-minimum" after seal removal) aimed at testing spontaneous colonisation and function recovery on a coarse technogenic substrate; (b) chopped cactus pear (*Opuntia ficus-indica* (L.)) cladodes and crushed asphalt (1:1 v/v) [CAOM], a low-input amendment intended to add labile organic matter and moisture retention while retaining the same on-site mineral matrix and natural-colonisation pathway as CA; (c) the upper 5 cm of asphalt were removed and replaced by 5 cm of Ap horizon from the adjacent Chromic Cambisol (Aric); *Sorghum bicolor* (L.) Moench var. Arcane was sown and surface irrigation was applied, followed by *Medicago sativa* L. [RA1], representing moderate-intensity rehabilitation through a thin "topsoil cap" and an annual-to-perennial vegetation sequence; and (d) the upper 5 cm of asphalt were removed and replaced by 5 cm of Ap horizon from the adjacent Chromic Cambisol (Aric); sterile commercial genotypes of *Chrysopogon zizanioides* (L.) Roberty were planted and surface irrigation was applied [RA2]. RA2 was conceived as an intentionally "boosted" benchmark to test the upper envelope of rapid root-driven structuring and biotic stimulation; however, because the deployment and long-term control of non-native (allochthonous) perennial grasses can be operationally and administratively challenging in real settings, RA2 is not intended as a generic recommendation for routine de-sealing projects. In qualitative terms, management intensity and expected implementation effort/cost increase as CA < CAOM < RA1 < RA2, with the main additional constraints being organic amendment handling (CAOM), access to suitable clean donor Ap material plus sowing/irrigation and early maintenance (RA1), and plant procurement plus containment/acceptability considerations for a non-native "booster" species (RA2). This ranking is deliberately qualitative, because actual costs depend strongly on local regulatory, logistical and agronomic conditions, including waste handling, donor-soil availability, irrigation needs, labour, and plant procurement. During the monitoring period, the delimited area was managed as a controlled-access research micro-site to minimise traffic and trampling artefacts. Vehicle passage and parking within the area were excluded, and pedestrian access was limited to scheduled operations (sowing/planting, irrigation checks and measurement campaigns). Operators approached plots from fixed access directions and avoided stepping on or across the de-sealed circles, particularly during wet conditions, so that observed changes in infiltration, compaction and biotic indicators primarily reflect treatment-driven recovery rather than repeated external disturbance.

On 6 November 2023, four additional 1-m-diameter plots were established, where, two days later (8 November 2023), hydroseeding was conducted using two leguminous species, namely *Medicago sativa* L. (ecotype Fontana murata) and *Scorpiurus muricatus* L. Within each circle, four rows were demarcated; two rows were sown with *M. sativa* and the remaining two with *S. muricatus*. For *M. sativa*, the seeding rate was 0.59 g per row. For *S. muricatus*, the seeding rate was 0.39 g per row. The subsequent surveys quantified overall vegetation cover, species-specific and weed-specific cover, the number of plants per row, and plant height.

2.1. Climatic and agrometeorological monitoring

Daily data for maximum temperature (T_{max}) and minimum temperature (T_{min}) and rainfall were provided by the Agro-Meteorological Information Service of the Sicily Region (SIAS) (http://www.sias.regione.sicilia.it/frameset_rete_new.htm, accessed November 2025). The standard weather station was installed near the experimental site (ID 276; 38°07′47.3″N 13°19′39.3″E) to collect, at hourly intervals, precipitation, P [mm], global solar radiation, Rs [W m^{-2}], air temperature, T [°C], air relative humidity, RH [%], wind speed [m s^{-1}] and direction [∘] at 2 m height.

2.2. Vegetation treatments and experimental layout

The red and yellow circles (treatments CA and CAOM) were left undisturbed, to allow natural vegetation to establish. In the green circles (treatment RA1), grain sorghum (*Sorghum bicolor* (L.) Moench) was sown on 23 March 2023 (Fig. 1).

The selected hybrid (var. Arcane; SIS sementi, Italy) was an early genotype with high tolerance to drought and disease. Fifty seeds were distributed in each de-sealed circle, to obtain (given a mean germination ability of 90%), a plant population of 45 plants (57 plants m^{-2}). In the blue circles (RA2 treatment), three vetiver (*Chrysopogon zizanioides* (L.)) tufts were transplanted on 28 March 2023. On the respective sowing and transplanting days, two square control plots, 1 m^2 each, were arranged outside the unsealed area and sown with the same plant species (hybrid *Sorghum* Arcane and vetiver), at the same plant populations used for the de-sealed areas. Plants were watered starting from the day after sowing (24 March 2023 for sorghum; 29 March 2023 for vetiver), distributing a water amount of 5 L $circle^{-1}$ (about 6.4 L m^{-2}), and checked at regular intervals (every 2 days until the end of March, and on a weekly basis in the following months, from sorghum plants' emergence to maturity and harvest).

After the first water supply, to ensure full plant establishment, individual plot management involved four successive irrigations to sorghum and two to vetiver. In sorghum, the applied water volumes were: 5 L $circle^{-1}$ (the first two waterings), 2.5 L $circle^{-1}$ and 3 L $circle^{-1}$, the last two waterings, respectively. In vetiver, 5 L $circle^{-1}$ were applied in the first watering, and 3 L $circle^{-1}$ in the second. For each de-sealed circle, the number of leaves per plant, plant height and SPAD index were recorded for all plants, performing 4 surveys from plants' emergence to full ripening. Sorghum panicles were harvested on 11 July 2023, and the number and weight of panicles were measured in all green seals and in the control. Furthermore, in all plots, including the controls, surveys were conducted for visual assessment of the degree of absolute and (only for the newly sown areas) specific vegetation covering, expressed as percentage (%) of soil area. Following the sorghum harvest, on 19 October 2023, a Sicilian landrace of alfalfa (*Medicago sativa*) known as "Fontana Murata" was sown in the same experimental plots. Prior to sowing, the soil was lightly tilled to a depth of 3–5 cm. The seeds were sown in rows spaced 15 cm apart, at a rate of 400 viable seeds per square metre (considering a germination rate of 85%). The surveys carried out concerned surface covered by vegetation (%) and the estimate of plant density (number of plants m^{-2}), for both parameters on the 30th day after sowing and after 548 days (in April 2025). In the initial phase of the experiment, for all plots from April to July 2023, monthly, the soil cover and the emergence of seedlings of all species (n° seedlings m^{-2}) were detected. Again, for all plots, surface covered by vegetation (%) and canopy height (cm) were monitored in April 2024 and 2025. Considering the encouraging growth observed across the initial four treatments, we undertook an additional trial: a set of linear cuts in the tarmac hydro-seeded with two herbaceous species—*Scorpiurus muricatus* and *Medicago sativa*. On 10 May 2024, height measurements were conducted for the newly sown plant species (*M. sativa* and *S. muricatus)*. A survey of floristic composition was carried out only in April 2025, following the phytosociological method of Braun-Blanquet, which also allowed the measurement of plant biodiversity level through the calculation of the Shannon Index (*H'*).

2.3. Beerkan infiltration measures

To determine the infiltration performance of the different treatments, Beerkan infiltration runs were conducted at two time points. In March 2023, one week after asphalt removal from the plots, and on 20 September 2024, approximately 18 months after de-sealing. In each campaign, one Beerkan run was performed in each circular plot (4 treatments × 4 plots = 16 runs), over two consecutive days.

We used a small-diameter metal ring (internal diameter 0.08 m)

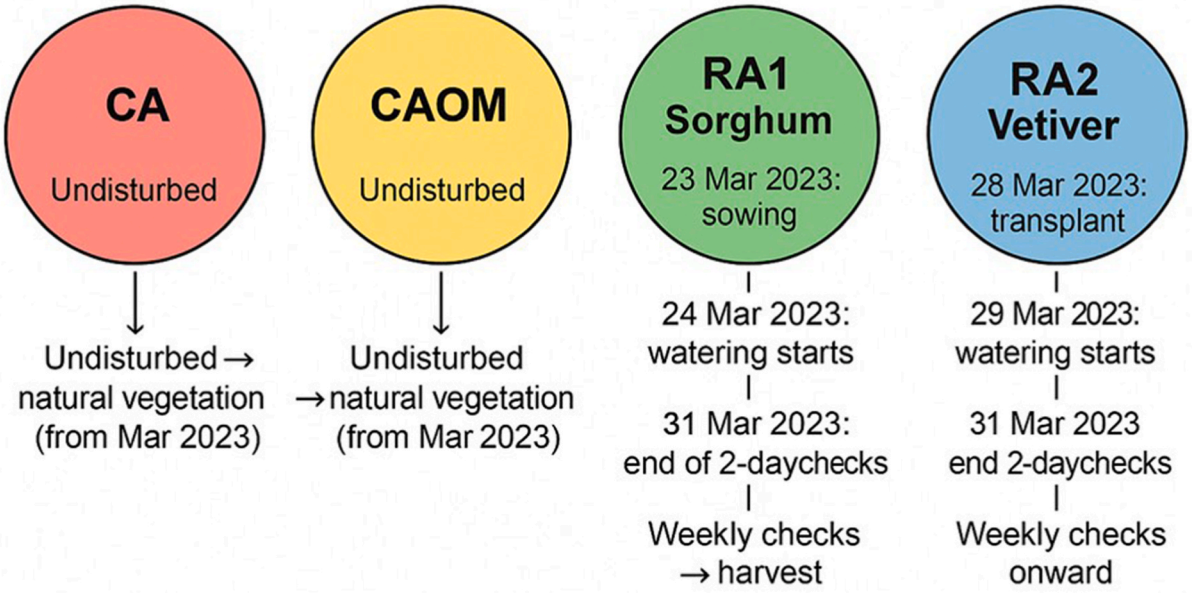

Fig. 1. Chronology of vegetation treatments. Red (CA) de-sealed soil left completely undisturbed from March 2023 to allow spontaneous vegetation. Yellow (CAOM): de-sealed soil amended with organic matter, then likewise left undisturbed for natural vegetation from March 2023. Green (RA1 – Sorghum): grain sorghum 'Arcane' sown 23 Mar 2023; watering began 24 Mar 2023; intensive checks every 2 days until 31 Mar 2023, followed by weekly checks until maturity and harvest. Blue (RA2 – Vetiver): three vetiver (*Chrysopogon zizanioides* (L.)) tufts transplanted 28 Mar 2023; watering began 29 Mar 2023; first check after 2 days (31 Mar 2023), weekly checks thereafter.

inserted into the Technosol surface to a depth of 0.01 m, following the Beerkan protocol (Lassabatère et al., 2006). The rings were inserted manually or with a rubber hammer, ensuring that the upper rim remained horizontal. A small ring was required because the surface layer was highly stony, making it difficult to conduct measurements over larger areas.

For each run, 25 equal water volumes of 140 mL were successively poured onto the confined infiltration surface. Each volume produced an initial ponded water depth of approximately 28 mm inside the ring. For every volume (1st–25th), we recorded the time from water application to complete infiltration, then applied the next volume (Bagarello et al., 2021; Lassabatère et al., 2006). To minimise surface disturbance by kinetic energy, water was poured from only a few centimetres above the surface and allowed to flow over the operator's fingers.

From the cumulative infiltrated depth (I) and corresponding times, we computed the instantaneous infiltration rate ($i_{r\text{-}f}$) at the end of each run. For each sampling point, a cumulative infiltration I (mm), vs. time, t (h), curve comprising 25 data points and the infiltration rates, i_r, at the end of the runs, $i_{r\text{-}f}$ (last value of i_r after applying all water volume) were obtained. Finally, the reduction rate, Δ, was calculated as a percentage ratio between the difference in $i_{r\text{-}f}$ values obtained in the first and the second sampling times and the $i_{r\text{-}f}$ values obtained from the first sampling time. This rate was then used as a clogging indicator. Details on full protocol, instrument specifications, calibration and QA/QC are reported in the SI.

2.4. Microbial sampling and enumeration

Asphalt and stones were collected directly from de-sealed areas by a surface buffering method, just after the soil unsealing. On September 12, 2023, a sterile zone for sample collection was established with a portable Bunsen's burner. A 2 × 2 cm square area was delimited on each sample by means of an aluminum square sampling template. The template was cleaned by submerging it in ethanol and sterilized by flaming before each sample collection. Using this fixed, sterilized template to delimit the sampled surface ensured a constant area for every swab, increasing precision and reproducibility of microbial counts compared with common swabbing methods that do not standardise the sampled surface. A 30 cm hand shovel was used with precision to carefully excavate the top 5 cm of the Technosol soil layer. Samples were then taken from the clean surface of a stone within the underlying soil layer, ensuring a minimum surface area of 2 cm^2. The internal area of the sampling template was swabbed using a sterile cotton swab (MEUS s.r.l, Pieve di Sacco, Padova, Italy) soaked in 4 mL of Ringer's solution. Each swab was then placed back into the test tube and stored in a portable fridge with reusable ice packs. Samples were collected in duplicate from each area. After collection, all samples were transported to the Agricultural Microbiology laboratory of University of Palermo and immediately subjected to microbiological analysis. Decimal dilutions of the samples were prepared in Ringer's solution. The samples were serially diluted using 1:10, 1:100, 1:1000 dilution factors in Ringer's solution. These cell suspensions were then used to estimate the total mesophilic count (TMC) on plate count agar (PCA), which was incubated aerobically at 30 °C for 72 h.

2.5. Spectroradiometric analysis and albedo estimation

We conducted an outdoor campaign on 11 December 2024 to characterise 16 de-sealed surface-cover samples and a shading transect near a building. Reflectance (ρ) measurements were collected with a field spectroradiometer using a calibrated white reference panel. The ρ measurements (SI) were used to derive the spectral signatures (350–2500 nm) of the selected samples; 20 replicates per sample were averaged to obtain the final signature. Water-vapour-affected wavelengths (1300–1450 nm) and $\lambda > 1800$ nm were excluded. Broadband albedo (α) for each sample was computed by integrating the mean spectrum. To assess building effects on illumination, $E_{\lambda i}$ was measured at 10 points along the transect (20 readings per point). Acquisition geometry (sensor–sun orthogonal, maximal standoff) minimized operator-induced reflections. Full protocol, instrument specifications, calibration and QA/QC are in the SI.

2.6. Soil CO_2 efflux measurements

The measurement chamber was 15 cm in diameter and 20 cm high, with a wall thickness of 0.3 cm, yielding a headspace volume of 3.5 L. Six measurement campaigns were conducted at approximately 80-day intervals after de-sealing. Collars of the same diameter and 10 cm height were permanently installed in each plot. CO_2 flux was measured using a JK40-M2-D infrared gas detector with built-in pump sampling (details in the SI). The instrument includes temperature compensation over a range of −40 to 70 °C, automatic zero tracking to prevent long-term drift, and three-point calibration to ensure measurement linearity and accuracy. A Wi-Fi interface was used to configure key measurement parameters and store data on a portable device (details in the SI).

2.7. Estimation of compaction and porosity dynamics from penetrometer resistance

Dynamic cone penetrometer (DCP) tests were conducted on 16 October 2023 and 10 April 2025 using a hand-driven standard device (8 kg drop mass, 575 mm drop height) to obtain continuous penetration resistance down to ≈0.85 m (deeper where feasible) in de-sealed and reference spots. Blow counts (mm blow^{-1}, DPI) were converted to California Bearing Ratio (CBR) and then to static soil cone penetration resistance (SCPR, qd) using published correlations (e.g. Langton, 1999; Gourves and Barjot, 1995). Resulting SCPR profiles (MPa) were used to identify compacted layers relative to literature threshold ranges for root limitation.

De-sealing on 7 March 2023 is taken as day 0. Sorghum was sown in every RA1 plot on day 16, and the first establishment irrigation followed on day 17; vetiver was transplanted into each RA2 plot on day 21, with the first irrigation supplied on day 22. Sorghum grew through the spring and was harvested on day 126. Microbial sampling of the Technosol surfaces was performed on day 189. After light surface tillage the RA1 circles were re-sown with alfalfa on day 226. Four additional circles were prepared on day 244 and hydroseeded two days later (day 246) with a mixture of alfalfa and *Scorpiurus*. Routine vegetation monitoring began in April 2024 (about day 405) and a detailed canopy height survey followed on day 430. The second Beerkan infiltration campaign, 18 months after de-sealing, fell on day 558. Spectroradiometric measurements for albedo determination were taken on day 645, and the final comprehensive vegetation and biodiversity survey was completed in mid-April 2025, around day 770.

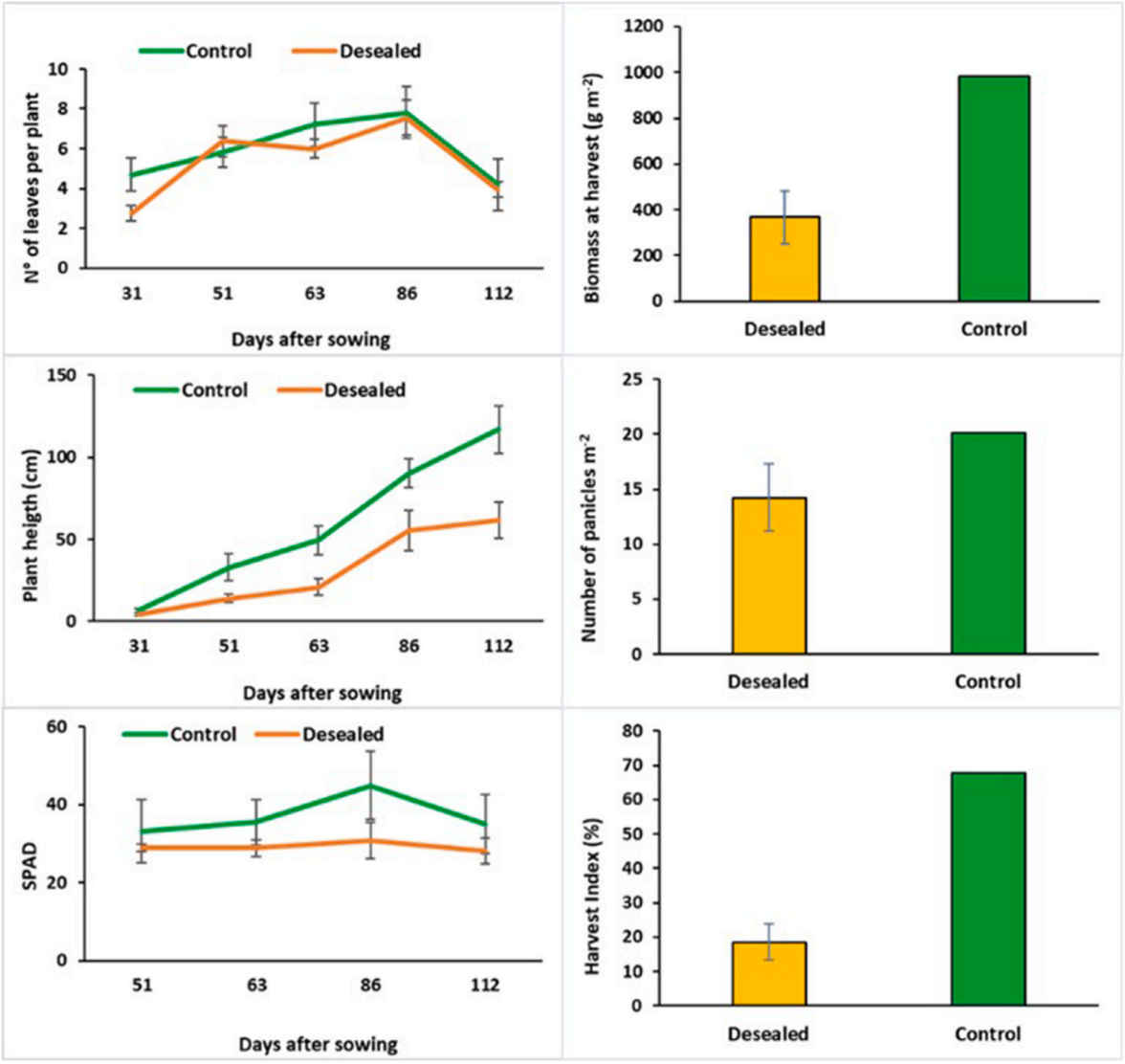

Fig. 2. Responses of *Sorghum bicolor* var. Arcane to de-sealing over time: Left-hand panel – time course: (top) number of leaves per plant, (middle) plant height and (bottom) leaf chlorophyll content (SPAD index), recorded from emergence to harvest. Right-hand panel – harvest traits: (top) total biomass, (middle) number of panicles, (bottom) harvest index. All values (except for the control) are means ± SD of independent plots.

2.8. Data processing and statistical analyses

All data were analysed using Minitab 19.1.1.0 (State College, PA, USA) for Windows. After checking the assumptions of residual normality and homogeneity of variance, plant data collected at harvest were analysed by one-way analysis of variance (ANOVA) according to the experimental design (Table SI). When the ANOVA was significant, pairwise differences among treatments were assessed using Fisher's LSD or Tukey's HSD test, depending on the dataset, at $p < 0.05$.

3. Results

3.1. Vegetation establishment and cover dynamics in de-sealed plots

Sorghum established rapidly in all plots, but plants grown in the de-sealed circles were consistently shorter and less productive than those in the unsealed control (Fig. 2). Sorghum seedlings emerged approximately 7 days after sowing, with no notable differences in emergence timing between de-sealed and control plots. However, consistent treatment effects were observed across all measured parameters, particularly in plant height and, to a lesser extent, SPAD chlorophyll index values (Fig. 2; table SI). At harvest, plants in the de-sealed plots were significantly shorter and less productive than those in the control, with reduced yields attributable to both a lower panicle density and decreased individual panicle weight (data not shown). Consequently, the harvest index (HI %) was also markedly reduced in the de-sealed plots compared to the control (Fig. 2; table SI). If plant roots primarily explore only the de-paved volume—approximately 235 dm^3 per planting circle (noting that roots may also grow beneath paved surfaces and to greater depths)—we can estimate the explored soil volume based on plant size. A 20 cm tall sorghum plant can explore a soil volume of approximately 20–30 dm^3 (Myers, 1980). With at least 10 plants per circle, the total volume explored would be between 200 and 300 dm^3. Therefore, the volume explored by roots would be not less than 85% of the de-paved volume.

The following two years of observations, 2024-25, showed pronounced differences in vegetation cover and canopy development among the four treatments (CA, CAOM, RA1, RA2), reflecting contrasting establishment pathways and species compositions (Fig. 3). In 2024, RA2 (vetiver) achieved the greatest total vegetation cover (83%) and the tallest canopy (74 cm). In contrast, CA and CAOM—both relying on spontaneous (natural) colonisation over crushed asphalt surfaces (with and without cactus cladode amendment, respectively)—displayed much lower total cover (12% and 17%) and shorter vegetation (15 cm and 20 cm). By 2025 all treatments increased in both cover and height, indicating progressive community development and stabilisation. Braun–Blanquet surveys (Fig. SI; Ttable SI2) show that the vegetation is dominated by herbaceous annual and perennial species. *Sonchus tenerrimus* L. was the most frequent and abundant taxon, recorded in nearly all plots with cover–abundance scores from "+" to "2", demonstrating strong site adaptation. *Erodium malacoides* and *Mercurialis annua* were also very frequent components of the emerging flora. Furthermore, Shannon Index (H') values ranging from 1.10 to 2.25 were calculated, which indicates moderate overall floristic diversity between the surveys.

3.2. Vegetation establishment in narrow linear tarmac cuts

Hydroseeding of *Scorpiurus muricatus* and *Medicago sativa* in narrow linear tarmac cuts produced rapid establishment and multi-year persistence, indicating that micro-de-sealing corridors can sustain vegetation even with minimal disturbance (Fig. 4). After 60 days both species were well established, with mean heights approximately 20 cm for *S. muricatus* and 16 cm for *M. sativa*. Applying the Myers (1980) framework for early (~60-day) explorable soil volume, *Scorpiurus* had occupied about 93% of its 0–30 cm half-cylindrical rooting volume, whereas *Medicago* had explored roughly 59% of its corresponding volume. Remarkably, both species persisted in the artificial asphalt cuts two years later. By the third year, only one *Medicago* plant remained across the four replicates.

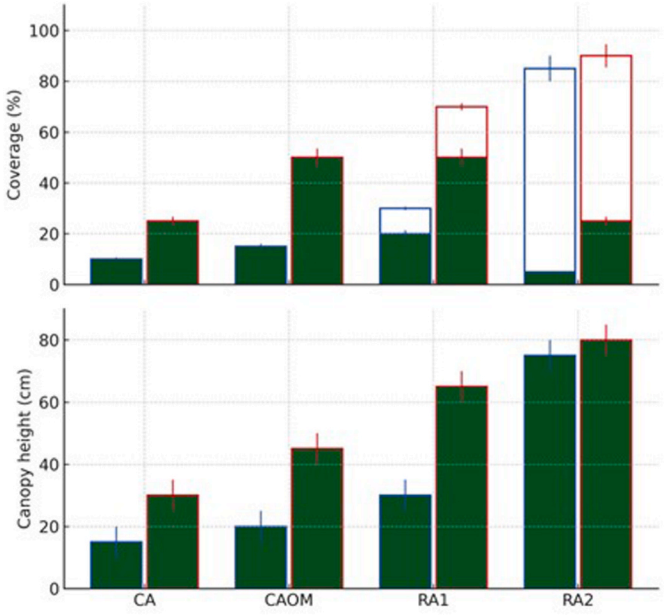

Fig. 3. Coverage and canopy development under four surface treatments: crushed asphalt (CA), chopped cactus pear cladodes + crushed asphalt (1:1 v/v) (CAOM), partial asphalt removal + 5 cm Cambisol Ap horizon with *Sorghum bicolor* followed by *Medicago sativa* (RA1), and partial asphalt removal + 5 cm Cambisol Ap horizon with *Chrysopogon zizanioides* (RA2). Bars show data from 2024 (blue outlines) and 2025 (red outlines). In the upper panel, weed (non-target) coverage is the closed dark-green portion; specific (target/introduced) vegetation coverage is the open portion stacked above. Canopy height (lower panel) is total vegetation height. Error bars indicate the standard error of each mean.

3.3. Infiltration behaviour of the four de-sealing treatments

Steady-state Beerkan infiltration rate was initially extremely high and similar across treatments, but after 18 months it declined and clearly differentiated between unvegetated and vegetated surfaces (Fig. 5; Table SI). At the first sampling time, Beerkan runs were very fast for all treatments, with total run durations between 0.02 and 0.21 h (Fig. 5) and the quasi steady-state Beerkan infiltration rates ($i_{r\text{-}f}$) (final rate at the end of each run) were reached quickly. The $i_{r\text{-}f}$ values (Table SI) were broadly comparable among treatments, suggesting that the differences in surface management did not influence soil hydraulic responses immediately after de-sealing. Moreover, the steady-state infiltration rate was far higher than the typical infiltration rate of structured mineral soils and closer to that of clean, coarse aggregates, suggesting that immediately after asphalt removal the surface behaved as a highly permeable, structureless Technosol.

At the second sampling time, Beerkan run durations were longer for all treatments, ranging from 0.04 to 2.79 h (Fig. 5) and treatment effects on $i_{r\text{-}f}$ became evident. A marked contrast emerged between unvegetated (CA, CAOM) and vegetated (RA1, RA2) surfaces: vegetated rehabilitation plots showed $i_{r\text{-}f}$ values lower than the unvegetated plots. Thus, by 18 months after de-sealing, the four treatments displayed clearly differentiated steady-state infiltration behaviour.

Across treatments, $i_{r\text{-}f}$ declined by 25–97% relative to initial values over 18 months. In CA and CAOM, the decline was moderate (Δ = 25–35%), consistent with continued infiltration through a coarse, weakly structured surface layer dominated by crushed asphalt. In contrast, RA1 and RA2 exhibited much stronger declines in $i_{r\text{-}f}$ (Δ =

Fig. 4. Top: Overhead view (1 m diameter white circle) of the single linear tarmac cut hydro-seeded with two forage species. Bottom: side views—left *Scorpiurus muricatus*, right *Medicago sativa*.

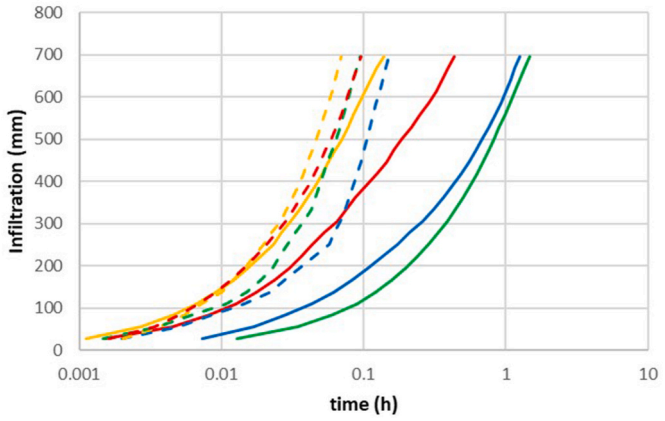

Fig. 5. Cumulative infiltration (mm) vs. time (h, log scale) for four surface treatments over two consecutive years. Red: CA (crushed asphalt); Yellow: CAOM (1:1 chopped cactus cladodes + crushed asphalt); Green: RA1 (top 5 cm asphalt replaced by 5 cm Ap horizon soil; *Sorghum bicolor* then *Medicago sativa*); Azure: RA2 (top 5 cm asphalt replaced by 5 cm Ap horizon soil; *Chrysopogon zizanioides*). Dotted lines represent the first year, whereas solid lines represent the second year.

89–97%) and longer run durations, indicating a transition toward hydraulic behaviour more similar to that of structured soils. In CAOM, the addition of chopped cactus cladodes may have enhanced retention of fine particles relative to CA, further contributing to the observed moderation of infiltrability (Table SI2). Overall, the reduction of steady-state final infiltration rates shows a consistent trajectory from initial hyper-permeability towards more regulated, soil-like behaviour, strongly modulated by the chosen de-sealing treatment.

3.4. Microbial colonisation of newly formed Technosols

The results of the microbiological counts are presented in Fig. 6. The one-way ANOVA revealed a significant effect of treatment on microbial load, $F(4,31) = 11.32$, $p < 0.001$. Post-hoc comparisons using Fisher's LSD test were then conducted to identify specific differences between groups. Surface microbial loads were higher in all de-sealed treatments than in the sealed control, with the highest values under RA2 (vetiver) (Fig. 6). The microbial load varied among treatments: the highest mean value ($\approx$4.0 $\log_{10}$ CFU cm^{-2}) occurred in RA2, while the lowest was in the control (C) at $\approx$2.0 $\log_{10}$ CFU cm^{-2}. RA2 differed significantly from RA1, CA, CAOM and C (Fisher's LSD, $p \leq 0.05$). RA1 (sorghum → alfalfa sequence), CA (crushed asphalt), and CAOM (1:1 chopped cactus cladodes + crushed asphalt) showed intermediate mean values ($\approx$3.2–3.6 $\log_{10}$ CFU cm^{-2}) that did not differ significantly from each other, but each was significantly higher than the control.

3.5. Spectral reflectance and albedo of treatment surfaces

Spectral signatures and derived albedo clearly distinguished asphalt from vegetated surfaces, with vegetation signals evident on colonised asphalt and weaker/altered patterns where vegetation was dry (Fig. 7; Table 1). Average spectral signatures were compared for selected characteristic samples, including reference asphalt (sample 2), reference vegetation, and CA and RA2 (covering plot 6 and 7, respectively)

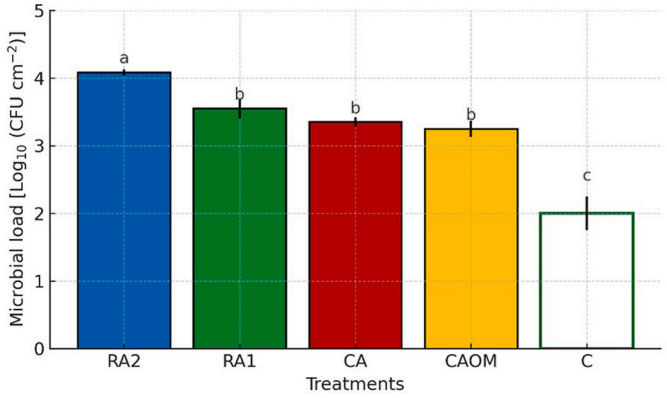

Fig. 6. Microbial loads (log_{10} CFU cm^{-2}) for surface treatments (means ± SE). Bars sharing a letter are not significantly different (Fisher's LSD, $p \leq 0.05$). Colours: RA2 (blue), RA1 (green), CA (red), CAOM (yellow), C (open bar with dark-green outline). Treatments: RA2 = rehabilitated surface (top 5 cm asphalt replaced by 5 cm Ap horizon soil) planted with sterile vetiver (*Chrysopogon zizanioides*); RA1 = rehabilitated surface (top 5 cm asphalt replaced by 5 cm Ap horizon soil) sown with *Sorghum bicolor* then *Medicago sativa*; CA = crushed asphalt; CAOM = 1:1 (v/v) chopped cactus cladodes + crushed asphalt mixture; C = control (reference surface).

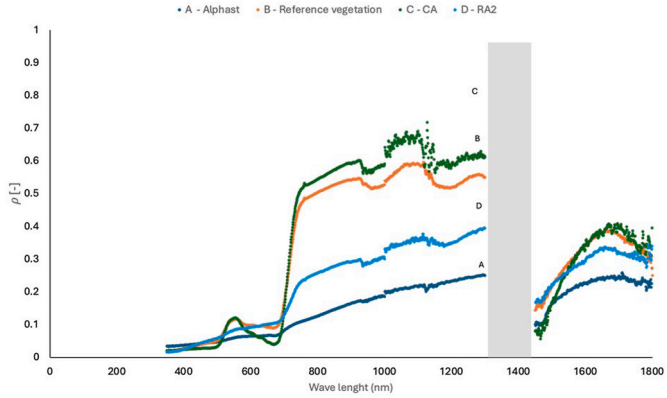

Fig. 7. Spectral signatures of selected samples asphalt (a), reference vegetation (b), CA (c) and RA2 (d). The grey box highlights the wavelength range 1300 – 1450 nm affected by noise due to atmospheric water vapour.

Table 1
Average broadband albedo values for the analysed surfaces.

Surface	Albedo (α)
asphalt	0.16
asphalt with vegetation	0.25
reference vegetation	0.35

(Fig. 7).

The asphalt spectrum shows no reflectance peaks at specific wavelengths in the visible spectrum (400–700 nm); reflectance values (ρ) are low (≈0.1–0.2). In the NIR (700–1300 nm), reflectance is slightly higher (≈0.2–0.3), consistent with the dark colour and absorptive properties of asphalt. The reference vegetation shows a peak around 550 nm and another around 700 nm, which corresponds to typical vegetation behaviour driven by chlorophyll absorption and the red edge.

The CA sample (Fig. 7c) shows reflectance peaks in the visible spectrum around 550 nm and 700 nm. In this sample, reflectance values are higher (≈0.2) and shifted between 570 and 600 nm (green–yellow), and NIR reflectance is around 0.5, consistent with the presence of healthy vegetation on the surface. In contrast, RA2 (Fig. 7d) does not display the typical vegetation patterns although NIR reflectance is around 0.5, indicating the presence of dry vegetation with reduced photosynthetic activity. The wavelength range 1300–1450 nm is affected by atmospheric water vapour noise (Fig. 7).

3.5.1. *Solar irradiation measurements along the transect*

Irradiance spectra along the transect confirmed a strong gradient from shaded to sunlit points, documenting the alteration of lighting conditions across the circles (Fig. 8). Irradiance was measured at each point along the transect as Eλi (W m^{-2} nm^{-1}), representing the radiant energy available at wavelength λ at point i. The analysis of the 10 points (Fig. 8) reveals a peak around 500 nm, where atmospheric transmittance is highest, and two minima around 900 nm and 1120 nm. This behaviour is due to atmospheric transmittance, which reaches ~60% at 900 nm and slightly above 30% at 1120 nm (Boyd and Petitcolin, 2004). The grey box shows the wavelength range 1300–1450 nm, where atmospheric transmittance is effectively zero, blocking the passage of electromagnetic waves from the light source. The amount of energy increases from the shaded area (bottom yellow curve) to the directly illuminated point (top cyan curve), confirming the effect of building-cast shading.

3.5.2. *Albedo analysis*

Broadband albedo increased from asphalt (0.16) to asphalt with vegetation (0.25) and reference vegetation (0.35) (Table 1). For each surface type, average spectral signatures were used to calculate albedo to characterise radiometric behaviour. The albedo values shown in Table 1 are in line with those reported by Zaragoza Ramírez and Bartolomé Muñoz, 2012, supporting the reliability of the measurements. Specifically, the lowest value refers to asphalt, suggesting that this surface limits reflection of solar energy. Similar values were obtained for asphalt with vegetation and reference vegetation, with a difference of ~0.10 likely linked to different lighting conditions of the circles.

3.6. *Soil CO_2 efflux and short-term carbon dynamics*

CO_2 efflux over the 700-day period was consistently higher in the vegetated rehabilitation treatments (RA1 and RA2) than in the crushed-asphalt treatments and the control (Fig. 9), indicating greater biological activity. The data presented in Fig. 9 and the post hoc comparisons (Table 2) highlight clear differences in CO_2 flux among treatments over the experimental period. Both the bar chart and time series show that RA1 (sorghum → Medicago sequence) and RA2 (vetiver) produced

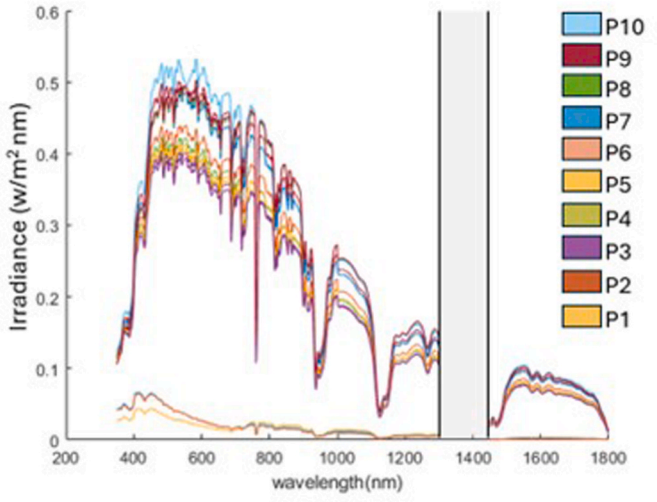

Fig. 8. Solar irradiance measured at 10 points placed along the transect. The grey box highlights the wavelength range (1300 – 1450 nm) affected by noise due to atmospheric water vapour.

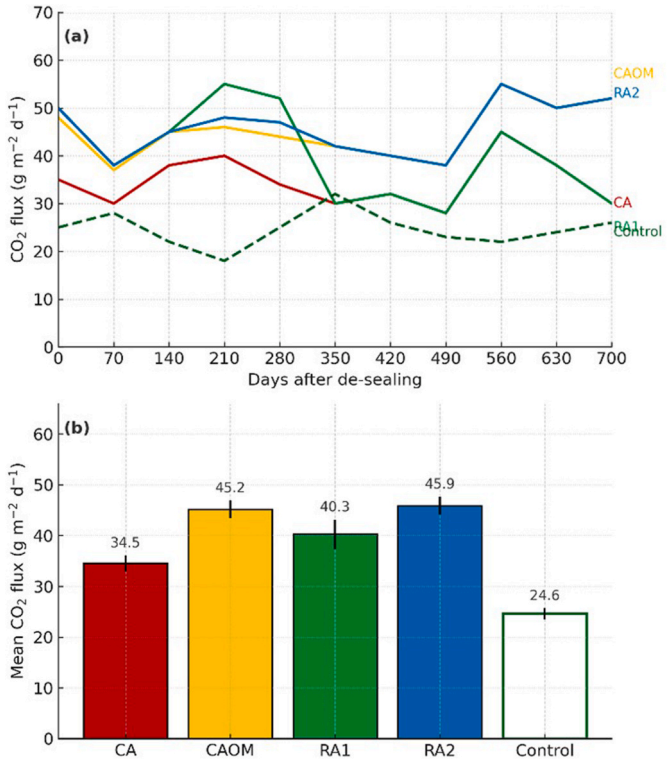

Fig. 9. (a) Temporal dynamics of CO_2 flux (g m^{-2} d^{-1}) over 700 days after de-sealing for treatments CA (crushed asphalt; red), CAOM (1:1 chopped cactus cladodes + asphalt; yellow), RA1 (rehabilitated soil with *Sorghum bicolor* → *Medicago sativa* sequence; green), RA2 (rehabilitated soil with vetiver *Chrysopogon zizanioides*; azure), and control (undeveloped reference; dark-green dashed). Lines are means of replications at each sampling date. (b) Mean (±SE) CO_2 flux across all sampling dates for the same treatments (control shown as open bar).

Table 2
Tukey HSD post hoc comparisons of CO_2 flux among treatments.

		Mean Difference	SE	df	t	p_{tukey}
CA	CAOM	−19.474	3.585	50	−5.432	<0.001
	CONTROL	−1.495	3.585	50	−0.417	0.993
	RA1	−17.030	3.585	50	−4.751	<0.001
	RA2	−20.239	3.585	50	−5.646	<0.001
CAOM	CONTROL	17.978	3.585	50	5.015	<0.001
	RA1	2.444	3.585	50	0.682	0.960
	RA2	−0.765	3.585	50	−0.214	1.000
CONTROL	RA1	−15.535	3.585	50	−4.334	<0.001
	RA2	−18.744	3.585	50	−5.229	<0.001
RA1	RA2	−3.209	3.585	50	−0.895	0.897

Note. P-value adjusted for comparing a family of 5 estimates.

higher CO_2 emissions compared to CA and CAOM and to the control.

These visual trends are confirmed by Tukey HSD tests (Table 2), which show statistically significant differences between the high-emission treatments (RA1 and RA2) and the lower-emission group, while no significant difference was observed between RA1 and RA2 themselves or between CA and the control.

3.7. Compaction dynamics assessed by soil cone penetrometer resistance

Subsurface compaction beneath the previously paved area relaxed markedly over 18 months, with PR in the 200–300 mm layer dropping from 7–16 MPa to 1–4 MPa, approaching the unpaved reference (Fig. 10). On 16 Oct 2023 (223 days after de-sealing), average PR in the 200–250 mm layer ranged from 7 to 15 MPa in all paved points,

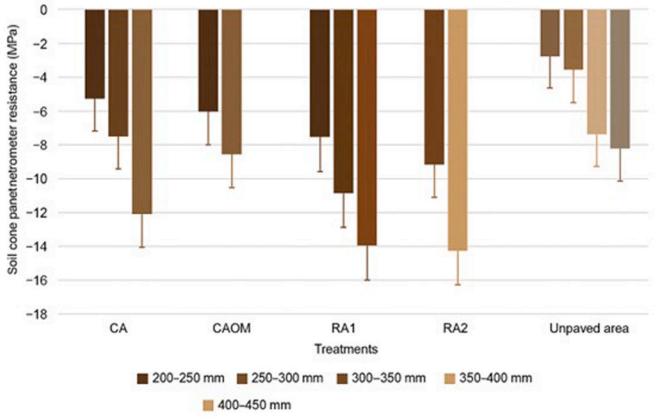

Fig. 10. Impact of de-sealing on the soil cone penetrometer resistance at different soil depths (in mm). Measurements after 223 (16 Oct 2023) and 765 (10 April 2025) days after de-sealing for CA (crushed asphalt), CAOM (1:1 chopped cactus pear cladodes + asphalt), RA1 (soil with *Sorghum bicolor* → *Medicago sativa*) and RA2 (soil with vetiver, *Chrysopogon zizanioides*). Bars indicate the mean soil cone penetrometer resistance at each depth, date and treatment; whiskers show ± standard error of the mean.

indicating a compacted layer at this depth, while it was 5 MPa in the unpaved area. On the same day, average PR in the 250–300 mm layer ranged from 13 to 16 MPa in the paved points (except CAOM), indicating a very compacted layer, while it was 4 MPa in the unpaved area. On 10 April 2025 (765 days after de-sealing), average PR in the 200–250 mm layer declined to 1–3 MPa in all previously paved points (2 MPa in the unpaved area). On the same day, the average value in the 250–300 mm layer declined to 1–4 MPa in the paved points (1 MPa in the unpaved area). Moreover, on 16 Oct 2023 the average PR in the unpaved area was 6 MPa at 300–350 mm, 8 MPa at 350–400 mm and 6 MPa at 400–450 mm; by 10 April 2025, average PR at 300–450 mm declined to <1 MPa in the unpaved area. Fig. 10 shows the impact of de-sealing on cone penetrometer resistance across soil layers 223 and 765 days after de-sealing for all paved points, compared to the unpaved area; the difference between average PR at day 765 and day 223 was computed for depth layers 200–250, 250–300, 300–350, 350–400 and 400–450 mm. Although literature threshold values for PR limiting root growth (1.5–4.2 MPa; Langton, 1999; Gourves and Barjot, 1995) were exceeded on day 223, roots still developed via macropores in the heterogeneous Technosol. Subsequent root development lowered PR by 6–15 MPa, indicating progressive loosening of soil structure in all previously paved points.

4. Discussion

Our results support a single core interpretation: micro-de-sealing triggers a coupled recovery trajectory in long-sealed Technosols, where hydro-physical structure, biotic functioning, and surface-energy properties co-evolve along a predictable sequence that is strongly modulated by surface design (substrate choice and vegetation). Immediately after seal removal, the system enters a short "hyper-permeability" phase; within ~18 months, infiltrability moderates while root activity and microbial colonisation increase; and by ~2 years, vegetation structure and surface albedo shift measurably, indicating the emergence of a functional soil–plant system with multiple regulating services.

The first stage is characterised by extremely high steady-state infiltration rates across all treatments, consistent with a structureless, coarse rubble layer created by asphalt removal and crushing (Fig. 5; Table SI). This initial hydraulic over-performance can buffer stormwater peaks, but it also implies a window of elevated preferential transport capacity if

soluble contaminants are present. By 18 months, steady-state infiltrability had declined by 25–97% relative to initial values and diverged among managements. This divergence is consistent with concurrent physical settling and fine infilling, together with biogenic aggregation and root-pore modulation, producing a shift from "instant drainage" toward more regulated, soil-like permeability (Sela et al., 2015). In practical terms, vegetation acted as a hydraulic regulator: it reduced excessive infiltrability that could limit plant-available water, while preserving infiltration capacity relevant to runoff mitigation.

In parallel with the hydraulic moderation, the sub-surface compaction legacy relaxed markedly, evidencing the second stage of the coupled trajectory: structural loosening associated with biological activity. Cone penetrometer resistance revealed an initially compacted layer at 200–300 mm depth beneath de-sealed plots (average PR ~7–16 MPa), followed by a decline to ~1–4 MPa over ~18 months, approaching ranges more favourable for root growth and biota movement (Fig. 10). The convergence of PR toward values measured in the unpaved reference area indicates that even minimal-disturbance interventions can re-establish functional pore networks on short timescales, aligning with reports of rapid biophysical recovery after de-sealing without extensive topsoil import (Maienza et al., 2021). Critically, the hydraulic trajectory (declining infiltrability) and the mechanical trajectory (declining PR) are not contradictory: together they indicate a transition from coarse, unstable macroporosity toward a more organizsd pore system shaped by settling, aggregation, and rooting.

Vegetation establishment and biological indicators form the third stage, explaining much of the treatment separation in functional outcomes. Canopy development differed sharply by treatment in the second year: vetiver (RA2) achieved the greatest cover and canopy height, whereas CA and CAOM—relying on spontaneous colonisation over crushed asphalt—lagged substantially before later gains (Fig. 3). Root exploration estimates indicate that early sorghum stands in RA1 could exploit a large fraction of the de-paved volume, showing that even small circular interventions can generate substantial rhizosphere development and initiate carbon and nutrient cycling. The successful establishment of herbaceous species in the linear asphalt cuts further supports micro-de-sealing as a scalable tactic to stitch vegetated corridors into sealed matrices (Fig. 4), with implications for shading and evapotranspirative cooling (Xiao et al., 2020).

Microbial and respiration data corroborate rapid reactivation of soil biological functioning after de-sealing. Vetiver (RA2) had the highest microbial load, while other treatments showed intermediate values, all higher than the control, confirming vegetation-driven stimulation of microbial activity (Fig. 6). These data reflect that rhizosphere processes and root exudation support microbial assembly, consistent with evidence that de-sealed Technosols can rapidly regain fertility (Chen et al., 2021; Maienza et al., 2021). Elevated values in CAOM indicate improvements even without intensive intervention. Sealed soils, instead, showed reduced microbial abundance and activity due to limited organic inputs (Renella, 2020).

CO_2 efflux further separated biologically engineered surfaces from inert ones: RA1 and RA2 showed higher fluxes than CA, CAOM and the sealed control (Fig. 9; Table 2), indicating intensified microbial metabolism and root activity—key markers of renewed carbon cycling formerly dampened under impervious cover (Anderson and Domsch, 1978a, 1978b). Interpreted within the coupled trajectory, elevated respiration plausibly reflects a transitional phase where recovery is accompanied by higher mineralisation; longer-term monitoring is needed to determine whether carbon accrual via biomass inputs and aggregation ultimately outpaces mineralisation, shifting the Technosol toward net storage.

Finally, spectral and albedo results show that the recovery trajectory is expressed not only belowground but also at the surface energy interface. Spectroradiometric signatures distinguished surface covers and support the measured increase in albedo from bare asphalt to asphalt–vegetation mosaics and reference vegetation (Fig. 7; Table 1). Together with restored infiltration and evapotranspiration, increased reflectance implies a plausible co-benefit for local heat-stress mitigation. The transect irradiance analysis highlights that building-induced shading can bias surface radiometry and validates the need for temporal replication under varying sun angles when coupling albedo to energy-balance modelling (Fig. 8).

From a design perspective, the coupled trajectory clarifies which levers most efficiently accelerate multifunctional recovery. Vegetation choice exerted strong leverage on simultaneous structural amelioration (PR decline), hydraulic moderation (controlled reduction in infiltrability), microbial rebound, and surface energy properties. Where intensive planting is infeasible, passive strategies (e.g., crushed asphalt retention) can still deliver meaningful gains relative to sealed controls, but with slower biological development and less moderation of infiltrability. Embedding time-explicit hydraulic and biotic benchmarks into de-sealing practice would also improve expectations management: early "over-infiltration" should be anticipated (and, where needed, managed with temporary sediment/contaminant controls), and subsequent performance targets should account for the predictable moderation phase. Interpreting the four treatments explicitly as a management-intensity gradient helps translate plot-scale outcomes into real deployment choices. CA operationalises the lowest-cost pathway (seal removal with maximal on-site reuse and minimal aftercare), suited to under-used paved areas where the primary target is rapid runoff buffering and where slower biological development is acceptable. CAOM adds a feasible, low-cost step—organic amendment using locally available biomass—intended to accelerate early biotic recovery and moisture buffering without the logistics of soil import, aligning with de-sealing programmes that promote pragmatic, modular actions and reuse (European Commission, 2012, 2013; Graie, 2018; Canino et al., 2020; Vieillard et al., 2024). RA1 represents moderate-intensity rehabilitation (thin Ap capping plus a crop-to-perennial sequence) and is likely the most transferable "assisted recovery" option where clean donor soil is available and establishment watering/maintenance can be guaranteed. RA2 should be read differently: it functions as an intentionally accelerated, upper-bound benchmark for what strong, deep rooting can accomplish within ~2 years, but it is not necessarily feasible or desirable as a standard practice because the use and long-term control of non-native (allochthonous) perennial grasses can be difficult under real-world regulatory and ecological constraints, even when sterile commercial material is used. Accordingly, the RA2 result primarily motivates the use of locally acceptable functional analogues (native or approved deep-rooted perennials) when the objective is to maximise coupled hydro-physical and biotic recovery while maintaining deployability and long-term governance.

Study limitations. This experiment is intentionally small-scale and nested within a single 15 × 5 m paved rectangle over one long-sealed Technosol, which constrains spatial generalisation but strengthens process-level inference by maximising comparability of initial conditions. Urban Technosols and fill materials can vary sharply over short distances; in that context, widely separated "replicates" may confound treatment contrasts with intrinsic substrate differences. We therefore replicated treatments within one well-defined soil body and treated each circular plot as the experimental unit (with subsamples averaged within plots). Accordingly, the values reported here should be interpreted as robust evidence of a coupled recovery trajectory for this specific setting rather than as city-wide averages. The same caution applies to the practical options tested here: they should be read as experimentally controlled intervention types rather than as a statistically representative sample of urban retrofitting practices. Additional limitations include the still short monitoring horizon for net carbon balance, potential pollutant mobilisation during the high-permeability window, and uncertainties in scaling across contamination loads, climates, and design geometries. Multi-site replication and longer-term tracking of infiltration, CO_2 efflux, spectral/albedo dynamics, and microbial community composition will be required to test the generality of the coupled trajectory and

to refine guidance on minimal yet effective interventions.

5. Conclusion

This mid-term field evidence shows that urban de-sealing triggers a rapid, coupled recovery of hydro-physical structure and biotic functioning in long-sealed Technosols. An initial phase of "hyper-permeability" follows seal removal, then a predictable decline toward moderated (yet still high) infiltrability within 18 months. Strategic vegetative rehabilitation (deep-rooted perennial and crop sequences) accelerates this transition, simultaneously reducing excessive infiltration rates, alleviating penetration resistance, increasing microbial biomass, and enhancing carbon cycling and albedo—thereby advancing multiple regulating ecosystem services (runoff mitigation, microclimate moderation, early biodiversity support). Passive or low-input treatments (e.g. crushed asphalt retention) still yield meaningful gains in microbial recolonisation and infiltration relative to sealed controls, offering cost-efficient options where intensive planting is constrained.

The study closes a knowledge gap on the temporal hydraulic trajectory of de-sealed urban soils by quantifying the staged permeability decline and linking it to structural and biological shifts. Recognising this trajectory enables more nuanced planning: anticipating early over-infiltration (and associated contaminant transport risks), timing vegetation establishment to harness settling and aggregation processes, and setting realistic performance benchmarks for stormwater and climate adaptation objectives. It also tempers the once axiomatic assumption that any de-sealing is uniformly and immediately beneficial, underscoring the need to characterise subsurface properties and manage the transition phase. With ~84 ha of new sealing added in 2023 (ISPRA, 2024) even as Palermo's draft urban plan mandates "zero new land consumption" via reuse of disused parcels (Comune di Palermo, 2024), de-sealing just 5 % of the city's under-used paved area (~50 ha) would both satisfy policy targets and unlock substantial hydrologic, climatic and ecological benefits. This de-sealing could infiltrate 10^5–10^6 m^3 extra stormwater annually, lower urban temperatures by ~0.1–0.2 °C (locally up to several °C), create habitat for dozens of species per hectare, and sequester 10^3–10^4 t of carbon over time.

Overall, de-sealing—when paired with judicious vegetation selection—emerges as a rapid, resource-efficient pathway to regenerate multifunctional urban soil systems. Embedding temporal hydraulic and biotic benchmarks into policy and design frameworks can enhance the effectiveness, cost efficiency, and resilience contributions of urban de-sealing initiatives aligned with climate adaptation, biodiversity enhancement, and sustainable stormwater management goals. From a planning perspective, these findings indicate that small, modular de-sealing interventions can be designed as effective "permeability islands" within highly sealed urban fabrics. Within less than two years, minimal-disturbance de-sealing restored rootable soil conditions, increased biological activity and delivered stable infiltration capacities that can be explicitly used as input for stormwater design and nature-based solutions. Treatments that combined asphalt removal with soil rehabilitation and vegetation establishment consistently outperformed options retaining crushed asphalt, suggesting that substrate choice and planting are critical design levers. Taken together, these results provide practical benchmarks and response times that can support municipalities and designers in prioritising de-sealing of under-used paved areas, operationalising "no net land take" targets and enhancing the climate resilience of Mediterranean cities. The multi-indicator protocol tested here could also contribute to the implementation of the recent EU Soil Monitoring Law by providing operational metrics for tracking de-sealing and soil function recovery in urban areas (European Parliament and Council of the European Union, 2025).

CRediT authorship contribution statement

Riccardo Scalenghe: Writing – review & editing, Writing – original draft, Visualization, Validation, Supervision, Resources, Project administration, Methodology, Investigation, Formal analysis, Data curation, Conceptualization. **Monica Auteri:** Writing – review & editing, Writing – original draft, Investigation, Formal analysis, Data curation. **Dario Autovino:** Writing – review & editing, Writing – original draft, Visualization, Methodology, Investigation, Formal analysis, Data curation. **Giorgio Baiamonte:** Writing – review & editing, Writing – original draft, Methodology. **Giacomo Belvisi:** Writing – review & editing, Writing – original draft, Investigation, Formal analysis, Data curation. **Chiara Cappadonia:** Writing – review & editing, Writing – original draft, Methodology, Investigation, Formal analysis. **Gaetano Caltabellotta:** Writing – review & editing, Writing – original draft, Investigation, Data curation. **Alessandra Carrubba:** Writing – review & editing, Writing – original draft, Visualization, Validation, Software, Methodology, Formal analysis, Data curation. **Giuseppe Ciraolo:** Writing – review & editing, Writing – original draft, Validation, Methodology, Investigation. **Antonio Comparetti:** Writing – review & editing, Writing – original draft, Methodology, Investigation, Data curation. **Giuseppe Di Miceli:** Writing – original draft, Resources. **Matteo Ippolito:** Writing – original draft, Methodology, Investigation, Data curation. **Dario De Caro:** Writing – review & editing, Investigation. **Massimo Iovino:** Writing – review & editing, Writing – original draft, Methodology. **Nicoletta Lala:** Writing – review & editing, Writing – original draft, Methodology, Investigation. **Santo Orlando:** Writing – review & editing, Investigation. **Filippo Saiano:** Writing – review & editing, Writing – original draft, Validation, Methodology, Investigation, Formal analysis, Data curation. **Mauro Sarno:** Investigation, Formal analysis. **Luca Settanni:** Writing – review & editing, Writing – original draft, Validation, Methodology, Investigation, Formal analysis, Data curation, Conceptualization. **Luciano Gristina:** Writing – review & editing, Writing – original draft, Visualization, Validation, Supervision, Methodology, Investigation, Formal analysis, Data curation, Conceptualization.

Declaration of competing interest

The authors declare that they have no known competing financial interests or personal relationships that could have appeared to influence the work reported in this paper.

Appendix A. Supplementary data

Supplementary data to this article can be found online at https://doi.org/10.1016/j.jenvman.2026.129845.

Data availability

All the data are included in the manuscript and Supplementary material.

References

Ajmone-Marsan, F., Biasioli, M., 2010. Trace elements in soils of urban areas. Water Air Soil Pollut. 213, 121–143. https://doi.org/10.1007/s11270-010-0372-6.

Ajmone-Marsan, F., Padoan, E., Madrid, F., Vrščaj, B., Biasioli, M., Davidson, C.M., 2019. Metal release under anaerobic conditions of urban soils of four European cities. Water Air Soil Pollut 230, 53. https://doi.org/10.1007/s11270-019-4101-5.

Anderson, J.P.E., Domsch, K.H., 1978a. Mineralization of bacteria and fungi in chloroform-fumigated soils. Soil Biol. Biochem. 10, 207–213. https://doi.org/10.1016/0038-0717(78)90098-6.

Anderson, J.P.E., Domsch, K.H., 1978b. A physiological method for the quantitative measurement of microbial biomass in soils. Soil Biol. Biochem. 10, 215–221. https://doi.org/10.1016/0038-0717(78)90099-8.

Aristegui, C.A., Perez, G.M.E., 2017. Soil sealing in Madrid (Spain), study case of Colmenar Viejo. Earth Sci. Res. J. 21, 111–116. https://doi.org/10.15446/esrj.v21n3.51450.

Bagarello, V., Caltabellotta, G., Iovino, M., 2021. Water transmission properties of a sandy-loam soil estimated with Beerkan runs differing by the infiltration time criterion. J. Hydrol. Hydromechanics 69. https://doi.org/10.2478/johh-2021-0010.

Boyd, D.S., Petitcolin, F., 2004. Remote sensing of the terrestrial environment using middle infrared radiation (3.0–5.0 μm). Int. J. Rem. Sens. 25, 3343–3368. https://doi.org/10.1080/01431160310001654356.
Calzolari, C., Tarocco, P., Lombardo, N., Marchi, N., Ungaro, F., 2020. Assessing soil ecosystem services in urban and peri-urban areas: from urban soils survey to providing support tool for urban planning. Land Use Policy 99, 105037. https://doi.org/10.1016/j.landusepol.2020.105037.
Canino, F., Cardinali, D., Marchi, N., Ricciato, P., Sambenedetto, G., Ungaro, F., 2020. Guidelines for the removal, management and Re-use of topsoil at construction sites. LIFE15 ENV/IT/000225. Available online: www.sos4life.it.
Chen, X.W., Wong, J.T.F., Wang, J.J., Wong, M.H., 2021. Vetiver grass-microbe interactions for soil remediation. Crit. Rev. Environ. Sci. Technol. 51, 897–938. https://doi.org/10.1080/10643389.2020.1738193.
Comune di Palermo, 2024. Piano Urbanistico Generale – documento Preliminare di Indirizzo. Verso il consumo di suolo zero, Urban Planning Department: Palermo, Italy. https://www.audis.it. (Accessed 20 December 2025).
Criado, M., Santos-Francés, F., Martínez-Graña, A., Sánchez, Y., Merchán, L., 2020. Multitemporal analysis of soil sealing and land use changes linked to urban expansion of Salamanca (Spain) using Landsat images and soil carbon management as a mitigating tool for climate change. Remote Sens. 12 (7), 1131. https://doi.org/10.3390/rs12071131.
Elvidge, C.D., Tuttle, B.T., Sutton, P.C., Baugh, K.E., Howard, A.T., Milesi, C., Bhaduri, B., Nemani, R., 2007. Global distribution and density of constructed impervious surfaces. Sensors 7, 1962–1979. https://doi.org/10.3390/s7091962.
European Commission, 2012. Guidelines on best practice to limit, mitigate or compensate soil sealing. SWD (2012) 101 final/2, European Commission: Bruxelles.
European Commission, 2013. Hard Surfaces, Hidden Costs - Searching for Alternatives to Land Take and Soil Sealing. Publications Office of the European Union, Luxembourg, p. 31. https://doi.org/10.2779/16427.
European Parliament and Council of the European Union, 2025. Directive on Soil Monitoring and Resilience (Soil Monitoring Law). Adopted at Second Reading by the European Parliament on 23 October 2025; Council first-reading Position: Position (EU) No 9/2025, OJ C/2025/5745, 28 October 2025.
Fini, A., Frangi, P., Mori, J., Donzelli, D., Ferrini, F., 2017. Nature based solutions to mitigate soil sealing in urban areas: results from a 4-year study comparing permeable, porous, and impermeable pavements. Environ. Res. 156, 443–454. https://doi.org/10.1016/j.envres.2017.03.032.
Fokaides, P.A., Kylili, A., Nicolaou, L.L., Ioannou, B., 2016. The effect of soil sealing on the urban heat island phenomenon. Indoor Built Environ. 25, 1136–1145. https://doi.org/10.1177/1420326X16644495.
García Alvarado, J.M., García Rodríguez, M.P., Pérez González, M.E., 2018. Evaluación y medida del sellado de suelos en el Norte de Madrid (España). Boletín de la Asociación de Geógrafos Españoles 76, 1–19. https://doi.org/10.21138/bage.2513.
García, P., Pérez, E., 2016. Mapping of soil sealing by vegetation indexes and built-up index: a case study in Madrid (Spain). Geoderma 268, 100–107. https://doi.org/10.1016/j.geoderma.2016.01.012.
Gourves, R., Barjot, R., 1995. The Panda ultralight dynamic penetrometer. In: Proceedings of the 11th European Conference on Soil. Mechanics and Foundation Engineering, Copenhagen, Denmark, 28 May–1 June 1995.
Graie, 2018. Métropole de Lyon. Ville Perméable. Actes de Conférence. http://www.graie.org/portail/conference-ville-permeable/ [in French].
Hopkins, K.G., Morse, N.B., Bain, D.J., Bettez, N.D., Grimm, N.B., Morse, J.L., Palta, M. M., Shuster, W.D., Bratt, A.R., Suchy, A.K., 2015. Assessment of regional variation in streamflow responses to urbanization and the persistence of physiography. Environ. Sci. Technol. 49, 2724–2732. https://doi.org/10.1021/es505389y.
Howard, J.L., Olszewska, D., 2011. Pedogenesis, geochemical forms of heavy metals, and artifact weathering in an urban soil chronosequence, Detroit, Michigan. Environ. Pollut. 159, 754–761. https://doi.org/10.1016/j.envpol.2010.11.028.
Howard, J.L., Dubay, B.R., Daniels, W.L., 2013. Artifact weathering, anthropogenic microparticles and lead contamination in urban soils at former demolition sites, Detroit, Michigan. Environ. Pollut. 179, 1–12. https://doi.org/10.1016/j.envpol.2013.03.053.
ISPRA, 2024. Consumo di Suolo, Dinamiche Territoriali e Servizi Ecosistemici. Rapporto SNPA 378/2024. Istituto Superiore per la Protezione e la Ricerca Ambientale, Rome, Italy. https://www.isprambiente.gov.it. (Accessed 20 December 2025).
IUSS Working Group WRB, 2006. World Reference Base for Soil Resources 2006, second ed. FAO, Rome, Italy, p. 132p. World Soil Resources Reports No. 103.
IUSS Working Group WRB, 2022. World Reference Base for Soil Resources, fourth ed. International Union of Soil Sciences (IUSS), Vienna, Austria, p. 234p.
Kabisch, N., Haase, D., 2013. Green spaces of European cities revisited for 1990-2006. Landsc. Urban Plann. 110, 113–122. https://doi.org/10.1016/j.landurbplan.2012.10.017.
Krówczyńska, M., Soszyńska, A., Pabjanek, P., Wilk, E., Hurbanek, P., Rosina, K., 2016. Accuracy of the soil sealing enhancement product for Poland. Quaest. Geogr. 35, 89–95. https://doi.org/10.1515/quageo-2016-0029.
Langton, D.D., 1999. The Panda light-weight penetrometer for soil investigation and monitoring material compaction. Ground Eng. 9, 1–16.
Lassabatère, L., Angulo-Jaramillo, R., Soria Ugalde, J.M., Cuenca, R., Braud, I., Haverkamp, R., 2006. Beerkan estimation of soil transfer parameters through infiltration experiments-BEST. Soil Sci. Soc. Am. J. 70. https://doi.org/10.2136/sssaj2005.0026.
Louise, A., Lucas, M., Adrien, T., Cyrille, V., Franck, R., 2024. After-sealing life in urban soils: experimental evidence of resilience and efficiency of ectomycorrhizal inoculation. Landsc. Urban Plann. 251, 105149. https://doi.org/10.1016/j.landurbplan.2024.105149.
Maienza, A., Ungaro, F., Baronti, S., Colzi, I., Giagnoni, L., Gonnelli, C., Renella, G., Ugolini, F., Calzolari, C., 2021. Biological restoration of urban soils after de-sealing interventions. Agriculture 11, 190. https://doi.org/10.3390/agriculture11030190.
Martinová, V., van Geel, M., Lievens, B., Honnay, O., 2016. Strong differences in *Quercus robur*-associated ectomycorrhizal fungal communities along a forest-city soil sealing gradient. Fungal Ecol. 20, 88–96. https://doi.org/10.1016/j.funeco.2015.12.002.
Myers, R.J.K., 1980. The root system of a grain sorghum crop. Field Crops Res. 3, 53–64. https://doi.org/10.1016/0378-4290(80)90007-6.
Nizeyimana, E.L., Petersen, G.W., Imhoff, M.L., Sinclair, H.R., Waltman, S.W., Reed-Margetan, D.S., Levine, E.R., Russo, J.M., 2001. Assessing the impact of land conversion to urban use on soils with different productivity levels in the USA. Soil Sci. Soc. Am. J. 65, 391–402. https://doi.org/10.2136/sssaj2001.652391x.
O'Riordan, R., Davies, J., Stevens, C., Quinton, J.N., 2021. The effects of sealing on urban soil carbon and nutrients. SOIL 7, 661–675. https://doi.org/10.5194/soil-7-661-2021.
Pabjanek, P., Krówczyńska, M., Wilk, E., Miecznikowski, M., 2017. An accuracy assessment of European soil sealing dataset (SSL2009): Stara Miłosna area, Poland - a case study. Miscellanea Geographica 20, 59–63. https://doi.org/10.1515/mgrsd-2016-0019.
Pérez, E., García, P., 2016. Monitoring soil sealing in Guadarrama River Basin, Spain, and its potential impact in agricultural areas. Agriculture 6, 7. https://doi.org/10.3390/agriculture6010007.
Peroni, F., Pristeri, G., Codato, D., Pappalardo, S.E., De Marchi, M., 2020. Biotope area factor: an ecological urban index to geovisualize soil sealing in Padua, Italy. Sustainability 12 (1), 150. https://doi.org/10.3390/SU12010150.
Pistocchi, A., Calzolari, C., Malucelli, F., Ungaro, F., 2015. Soil sealing and flood risks in the plains of Emilia-Romagna, Italy. J. Hydrol.: Reg. Stud. 4B, 398–409. https://doi.org/10.1016/j.ejrh.2015.06.021.
Prokop, G., Jobstmann, H., Schönbauer, A., 2011. Overview of best practices for limiting soil sealing or mitigating its effects in EU-27. Eur. Comm. DG Environ. https://doi.org/10.2779/15146.
Recanatesi, F., Petroselli, A., Ripa, M.N., Leone, A., 2017. Assessment of stormwater runoff management practices and BMPs under soil sealing: a study case in a peri-urban watershed of the metropolitan area of Rome (Italy). J. Environ. Manag. 201, 6–18. https://doi.org/10.1016/j.jenvman.2017.06.024.
Renella, G., 2020. Evolution of physico-chemical properties, microbial biomass and microbial activity of an urban soil after de-sealing. Agriculture 10, 596. https://doi.org/10.3390/agriculture10120596.
Rodríguez-Rojas, M.I., Huertas-Fernández, F., Moreno, B., Martínez, G., Grindlay, A.L., 2018. A study of the application of permeable pavements as a sustainable technique for the mitigation of soil sealing in cities: a case study in the south of Spain. J. Environ. Manag. 205, 151–162. https://doi.org/10.1016/j.jenvman.2017.09.075.
Romero Díaz, A., Caballero Pedraza, A., Pérez Morales, A., 2017. Urbanisation and tourism in the Campo Cartagena-Mar Menor area (Murcia, Spain). Impact on soil sealing. Cuad. Tur. 39, 521–546. https://doi.org/10.6018/turismo.39.290691.
Sandin, M., Jarvis, N., Larsbo, M., 2018. Consolidation and surface sealing of nine harrowed Swedish soils. Soil Tillage Res. 181, 82–92. https://doi.org/10.1016/j.still.2018.03.017.
Scalenghe, R., Ajmone-Marsan, F., 2009. The anthropogenic sealing of soils in urban areas. Landsc. Urban Plann. 90, 1–10. https://doi.org/10.1016/j.landurbplan.2008.10.011.
Sela, S., Svoray, T., Assouline, S., 2015. The effect of soil surface sealing on vegetation water uptake along a dry climatic gradient. Water Resour. Res. 51, 7452–7466. https://doi.org/10.1002/2015WR017109.
Siedentop, S., Fina, S., 2012. Who sprawls most? Exploring the patterns of urban growth across 26 European countries. Environ. Plann. 44, 2765–2784. https://doi.org/10.1068/a4580.
Stankovics, P., Tóth, G., Tóth, Z., 2018. Identifying gaps between the legislative tools of soil protection in the EU Member States for a common European soil protection legislation. Sustainability 10, 2886. https://doi.org/10.3390/su10082886.
Tardieu, L., Hamel, P., Viguié, V., Coste, L., Levrel, H., 2021. Are soil sealing indicators sufficient to guide urban planning? Insights from an ecosystem services assessment in the Paris metropolitan area. Environ. Res. Lett. 16 (10), 104019. https://doi.org/10.1088/1748-9326/ac24d0.
Ugolini, F., Baronti, S., Lanini, G.M., Maienza, A., Ungaro, F., Calzolari, C., 2020. Assessing the influence of topsoil and Technosol characteristics on plant growth for the green regeneration of urban built sites. J. Environ. Manag. 273, 111168. https://doi.org/10.1016/j.jenvman.2020.111168.
Vieillard, C., Vidal-Beaudet, L., Dagois, R., Lothode, M., Vadepied, F., Gontier, M., Schwartz, C., Ouvrard, S., 2024. Impacts of soil de-sealing practices on urban land-uses, soil functions and ecosystem services in French cities. Geoderma Reg. 38, e00854. https://doi.org/10.1016/j.geodrs.2024.e00854.
Xiao, R., Tian, Y., Xu, G., 2020. Spatial gradient of urban green field influenced by soil sealing. Sci. Total Environ. 735, 139490. https://doi.org/10.1016/j.scitotenv.2020.139490.
Zaragoza Ramírez, A., Bartolomé Muñoz, C., 2012. Energy, Engineering and Technologies - Manufacturing and Environment. In: Ghenai, C. (Ed.), InTech. https://doi.org/10.5772/29536.